Journal of Power Sources 260 (2014) 299–306

Contents lists available at ScienceDirect

Journal of Power Sources

journal homepage: www.elsevier.com/locate/jpowsour

High-performance/low-temperature-processed dye solar cell counter electrodes based on chromium substrates with cube-like morphology

Fatemeh Behrouznejad [a], Nima Taghavinia [a,b,*]

[a] Institute of Nanoscience and Nanotechnology, Sharif University of Technology, Azadi Avenue, Tehran, Iran
[b] Department of Physics, Sharif University of Technology, Azadi Avenue, Tehran, Iran

HIGHLIGHTS

- Cyclic electrodeposition of Pt on cube-like Cr films provides efficient counter electrodes.
- The rough Cr coating can be electro-deposited on large area with low cost.
- Highly dispersed Pt nanoparticle layer on defect sites and edges of Cr cubes is formed.
- R_{ct} as low as 0.27 Ω cm^2 and solar cell efficiency more than 9% is obtained.
- Cr and Pt depositions are made at low temperature, hence are suitable for flexible DSCs.

GRAPHICAL ABSTRACT

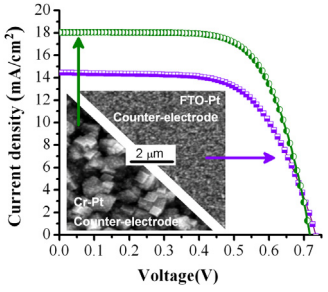

ARTICLE INFO

Article history:
Received 9 November 2013
Received in revised form
24 January 2014
Accepted 20 February 2014
Available online 20 March 2014

Keywords:
Dye sensitized solar cell
Counter electrode
Cube-like morphology
Charge transfer resistance

ABSTRACT

There is still an open question of how to prepare high-performance counter electrodes for dye solar cells (DSCs) at room temperature; a requirement for flexible DSCs. Here, we introduce Pt deposited cube-like chromium coating as a low-temperature highly-efficient counter electrode for DSCs. Cr is a chemically stable metal and can be easily electroplated on conductive substrates with high roughness (here ~160 nm) and cube-like appearance. A cyclic electrochemical deposition method with optimized temperature and number of cycles is used to grow Pt nanoparticles on this surface and charge transfer resistance as low as 0.54 Ω cm^2 and 0.27 Ω cm^2 were obtained at 40 °C and 55 °C solution temperatures, respectively. More surface defects (kinks, terraces and ledges) on the cube-like chromium film, as well as the electric field enhancement near the cube edges produces more dispersed Pt nanoparticles on this substrate compared to FTO (fluorine doped tin oxide) substrate. By replacing the conventional DSC counter electrode (thermal Pt on FTO) with this new electrode, filling factor and efficiency increase from 0.63–6.6% to 0.68–8.77%, without a scattering film. The efficiency can be as high as 9.52% by using a scattering film.

1. Introduction

Dye solar cells (DSC) include a photoanode consisting a dye adsorbed mesoporous layer of metal oxide nanoparticles (usually TiO_2 or ZnO) on a transparent conductive oxide (usually fluorine-doped tin oxide: FTO), a catalyst coated conductive layer (usually

* Corresponding author. Department of Physics, Sharif University of Technology, Azadi Avenue, Tehran, Iran. Tel.: +98 21 6616 4532; fax: +98 21 6602 2711.
E-mail address: taghavinia@sharif.edu (N. Taghavinia).

http://dx.doi.org/10.1016/j.jpowsour.2014.02.074
0378-7753/

platinum coated FTO) as a counter electrode and an electrolyte containing a redox couple (usually I^-/I_3^-) in between. By light absorption, electrons are injected from the excited dyes to the conduction band of metal oxide. The lack of electron in the dye molecule is compensated by oxidizing I^- to I_3^-, followed by the diffusion and reduction of I_3^- ions to I^- at the surface of counter electrode [1]. In the last decade, DSC has attracted attention due to comparatively low production cost and simplicity of fabrication. However, for large scale production and large size modules, the FTO/glass substrates are not favoured due to the high price and high sheet resistance. The FTO high sheet resistance leads to loss of the conversion efficiency (η), mainly by reducing the filling factor (FF).

Metal sheets have the advantage of lower price and better electrical conductivity; however, many of them are unstable in the aggressive DSC electrolyte. The conventional DSC electrolyte contains iodine as a major component, which is corrosive and prohibitive for using a wide variety of metals, either as substrates or as bus bars. Metals such as Cu [2], Al [2–4], Fe [4,5], Ag [3], Au [3], Zn [4,5], Pd [6] and also alloys such as carbon steel [5] are corroded in iodine electrolytes.

Several attempts have been so far made for replacing FTO of the counter electrode with metals, such as stainless steel foils [5,7–11], Ni foils [12], Ti sputtered layers [13,14], Ti foils [15], Ti mesh [16], submicron graphite [17] and other carbon materials (in monolithic DSCs [18–20] or conventional cells [21,22]). The aim is to reduce the cost of the cells and also decrease the series resistance which is very important in large cells or modules. Although using Ti mesh and foil reduces the series resistance of DSCs, it cannot considerably reduce the cost. In case of Ni and stainless steel, the issue of corrosion is still controversial; some believe that they are not stable [3,6,10,11,23,24] and should be used with a protective layer, and some have shown that they are stable even without any protective layer [5,7]. It has been shown by electrochemical impedance spectroscopy (EIS) that the corrosion resistance of stainless steel-304 decreases in the first 24 h [25].

Chromium is a chemically stable metal in corrosive media, due to a native compact oxide layer on its surface. It can also be easily electrodeposited over large scale conductive substrates with low cost. The morphology and surface roughness can be controlled by varying electrodeposition conditions. There is, however, no report so far on using electrodeposited chromium as a substrate for DSC counter electrode. Here in this paper we are evaluating chromium as the substrate of counter electrode.

Platinum is the usual electro-catalyst material used in the counter electrode of DSCs. Pt is chemically stable and shows the best catalytic activity for the reduction of triiodide ions. The catalytic activity of other materials is generally inferior; materials such as TiN nanotubes [26] WO_2 nanorods [27], Mo_2C and WC [28], Cr_3C_2, CrN, VC(N), VN, TiC, NiS [29], V_2O_3 [30], TaOx, Ta_3N_5, Ta_4C_3 [31], polymer materials [32,33] and carbon based materials [34,35] have been used as the catalyst of counter electrode. Among these, carbon materials and structures [22] have attracted more attention. A drawback for carbon coatings is the low adhesion to the substrates [34], and the large thickness (several micrometers) required in order to attain highly efficient cells [36].

Pt is conventionally deposited on FTO by thermal decomposition of a Pt salt, usually H_2PtCl_6. While this method provides well dispersed and highly adhering Pt nanoparticles on the surface [37], it cannot be used for plastic substrates, which do not tolerate thermal treatments. Methods such as physical vapour deposition (PVD, such as sputtering), chemical reduction, photochemical deposition and electrodeposition are introduced as low temperature processes for counter electrode. PVD method is too expensive and not economically favoured for large scale deposition. Chemical liquid-phase reduction methods on FTO/glass [38,39], ITO-PEN (indium tin oxide coated polyethylenenaphthalate) [40], Ni and stainless steel foil [12] have been tried; however, Pt nanoparticles by these methods are not generally well stable in DSCs [41], while it is claimed that in case of gas-phase reduction method, good adhesion is obtained [42]. Photo-platinization, using TiO_2 as a photo-catalyst, has been also reported. A disadvantage of this method is the high sensitivity of the product to the thickness of TiO_2 [43]. Among the low temperature Pt deposition methods, electrodeposition seems more versatile and promising.

An important factor in the performance of a counter electrode is the surface roughness, that is, the active catalytic area of the electrode. Generally two routs could be considered to control the roughness, i.e. controlling Pt deposition conditions, and utilizing rough substrates for Pt deposition.

Fang and co-workers indicated that by increasing the thickness of a Pt sputtered film from 2 nm up to 25 nm, the charge transfer resistance is decreased. The trend stops for thicker films where it becomes mirror-like [44]. Electrodeposition provides more parameters to control the morphology and the roughness, via different electrodeposition methods (constant current [45–47], constant voltage [48], pulse [45,49–52] and cyclic electrodeposition [53]). These depositions are done using Pt salts [45–47,49–52] or Pt nanoparticles [48]. There is controversy on the quality of electrodeposited Pt counter electrodes. Some believe that thermal decomposition method results in superior counter electrodes [45], while others claim that electrochemical deposition produces higher surface area and therefore higher photocurrent density [48–52]. Various deposition conditions and charge transfer resistance have been reported for these counter electrodes (ether deposited using thermal decomposition or electrodeposition). In the current research we first synthesize high performance counter electrodes using thermal decomposition (charge transfer resistance about 1.1 $\Omega\ cm^2$), which is used to compare with the electrodeposited counter electrodes. It has been shown that by a pulse current electrodeposition method, mono-sized Pt nanoparticles formation occurs, whereas in the direct current electrodeposition, dendritic growth occurs [47]. The pulsed electrodeposition method also provides greater surface area and higher chemical activity compared to the sputtering method [49]. A charge transfer resistance of about 8.4 $\Omega\ cm^2$ with transmission of 80% is reported for a FTO–Pt counter electrode that is deposited using pulse electrodeposition [50].

More elaborated methods such as using polystyrene [54] or TiO_2 [55] as a template or scaffold have been used to produce Pt films of higher active surface area [54]. The surface area of the deposited Pt can also be enhanced by using textured or rough substrates. For stainless steel foil, it has been shown that etching in acidic solutions enhances the quality of Pt counter electrode [12,56]. Similarly, texturing FTO substrates to increase the roughness has been reported very effective [57]. By changing the FTO roughness from 0.18 nm to 28.3 nm, Pt charge transfer resistance has decreased from 9.7 $\Omega\ cm^2$ to 4.55 $\Omega\ cm^2$, respectively [57].

Here in this paper, we introduce cube-like chromium coating as a rough coating with high chemical stability and low sheet resistance that provides high surface area for electrodeposition of Pt. High electric field strength at the edges of the Cr semi-cubes on the surface, as well as large surface defect density around the edges, seem to be critical for high performance Pt deposition, using cyclic electrodeposition at the controlled temperature.

2. Materials and methods

Cube-like Cr film deposition and characterization.

Chromium on FTO/glass substrates (15 $\Omega\square^{-1}$, Dyesol) was electrodeposited in a two electrode configuration. The electrodeposition solution contained chromic acid (CrO_3: 210 g L^{-1}) and

sulphuric acid (H_2SO_4: 2.1 g L^{-1}). The counter electrode for chromium electrodeposition was a Pb electrode and the solution temperature was 38 °C. The DC current to produce a cube-like surface on a 1 cm × 1.5 cm FTO substrate was 0.2 A. Cr films were deposited for 30 s, 60 s, 120 s and 240 s to investigate the effect of deposition time on the surface morphology. The samples were rinsed and Pt was electrodeposited right after Cr plating, to avoid formation of oxide layer. The stability of chromium was studied using Inductive Coupled Plasma atomic emission spectroscopy (ICP). The root-mean-square roughness (R_{rms}) of deposited Cr films was determined using Atomic Force Microscopy (AFM) images (Veeco-CP research). Diffuse reflection was carried out using an integrating sphere and an Avantes photospectrometer (Avaspec-2048TEC). Electron microscopy was performed using a Vega–Tescan machine in the backscattered electron mode.

2.1. TiO_2 photo-anode preparation

FTO substrates were $TiCl_4$ treated at 70 °C in a solution of 30 mM $TiCl_4$ (Merck) in DI water. The photo-anode film was produced by doctor-balding a transparent TiO_2 paste (Sharif Solar) composed of 20 nm TiO_2 nanoparticles, followed by a scattering film containing 150–250 nm TiO_2 particles (Merck). The pasted layers with the active area of 0.45 cm × 0.45 cm, were heat treated in the following sequence: 70 °C (30 min), 320 °C (15 min), 380 °C (15 min), 450 °C (15 min) and 500 °C (1 h). The films were again $TiCl_4$ treated. The thickness of the final transparent and scattering films was 17 μm and 4 μm. The electrodes were immersed in the dye solution (0.2 mM cis-di(thiocynato)-N,N′-bis (2,2′-bipyridyl-4-caboxylic acid-4′-tetrabutylammonium carboxylate)) ruthenium(II) (N719,Dyesol), for 20 h, then rinsed using an acetonitrile solution.

2.2. Pt deposition

For the conventional counter electrode, Pt is deposited by thermal decomposition method: a drop of 5 mM $H_2PtCl_6 \cdot 6H_2O$ in 2-propanol solution is spread on the surface of 1 cm × 1.5 cm substrate (FTO or Cr), followed by calcination in 450 °C. This is repeated for two times. Pt electrodeposition was performed using a cycling deposition method by a three electrode system: Ag/AgCl as a reference, Pt-coated FTO as a counter electrode and chromium-coated substrate as a working electrode. The plating solution contained 3 mM $H_2PtCl_6 \cdot 6H_2O$ and 50 mM KNO_3 in DI water. Bath temperature and number of deposition cycles were changed for optimization.

2.3. DSC assembling and characterizing

The cells were sealed using 60 μm thick syrlyn sheets (Dyesol) and filled with an electrolyte containing 30 mM I_2 (Merck), 100 mM LiI (Merck), 100 mM guanidinium thiocyanate (GSCN) (Merck), 1-butyl-3-methylimidazolium iodide (Aldrich) and 500 mM 4-tert-butylpyridine (TBP) in the acetonitrile and valeronitrile solvent (85:15 v/v). Current–voltage plots were recorded using a Palmsens potentiostat under AM1.5 simulated light (Sharif Solar). Electrochemical Impedance Spectroscopy (EIS) was carried out using Autolab potentiostat in frequency range 10^5 Hz down to 1 Hz.

3. Results and discussions

3.1. Cube-like Cr electrodeposited films

Chromium is a chemically stable metal in the aggressive iodine based DSC electrolyte due to a dense native oxide layer on the surface. Deposited Cr films show no sign of dissolution in the electrolyte: ICP measurement of Cr in the electrolyte with the cube-like Cr substrate immersed in shows no change of Cr concentration for about 6 days. In practice, a major advantage of Cr as a substrate is that it can be electrodeposited on large area conductive substrates with low cost. The roughness and morphology of the electrodeposited film is controllable by changing temperature, deposition current density and the additives of the plating solution,

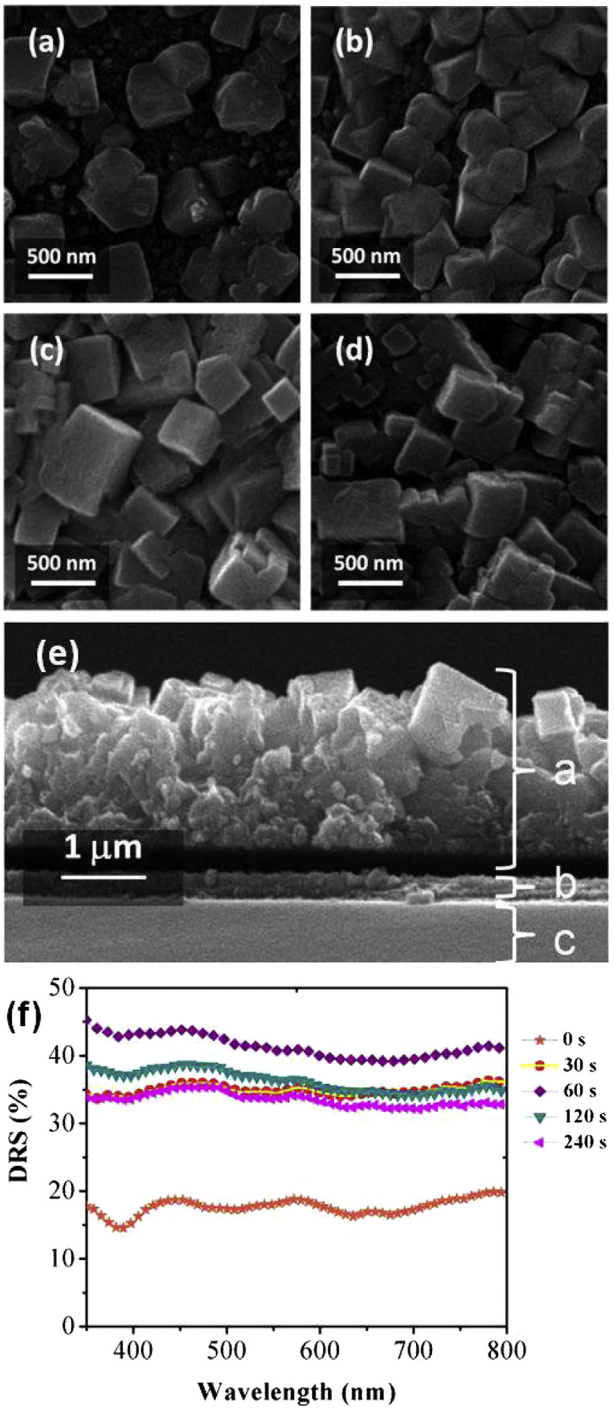

Fig. 1. SEM image of electrodeposited Cr film with constant current density (0.13 A cm^{-2}) and different deposition time: a) 30 s, b) 60 s, c) 120 s and d) 240 s. The cross-section of layers is illustrated in part e (e-a: Cr layer that is deposited using electrodeposition method, e-b: Conducting substrate, here FTO, and e-c: glass). Diffuse reflection spectra of these samples are also illustrated in this figure compared to a bare FTO surface (0 s) (f).

and the thickness can be controlled by monitoring the transferred charge. The morphology and DRS spectra for different deposition time are shown in Fig. 1. For deposition time of 30 s, some cube-like Cr particles are produced on the substrate. With increasing deposition time, the density of Cr-cubes increases. The largest cube size, as well as the highest DRS is obtained for deposition time of 60 s (Fig. 1c). After that, smaller cubes fill the free space between the large cubes, so DRS value will decrease. The deposition time of 120 s is selected in this research, due to lower electrical resistance and also relatively high DRS (about 40%) and roughness (~160 nm) values. In addition to optical effects, the high surface roughness of the cube-like morphology has direct effect on decreasing the charge transfer resistance at the counter electrode surface due to increasing the surface area. [12,41,49,54–57].

3.2. Pt deposition

3.2.1. Thermal Pt deposition

Pt is conventionally deposited on FTO/glass substrates using thermal decomposition method, i.e. by spreading a drop of H_2PtCl_6 solution on the surface, followed by heat calcinations. Fig. 2 shows SEM images of the surface of Pt-coated and uncoated FTO. Pt is a heavy element, so Pt nanoparticles produce more intense signal in the back scattered imaging mode. Comparing the morphology of FTO with cube-like Cr, it is clear that cube-like Cr is considerably rougher, that is, provides larger surface for Pt deposition.

Pt was similarly deposited on Cr substrates using thermal decomposition method. The FTO-Pt and Cr–Pt electrodes were used as the counter electrode of DSCs. The performances of the devices are displayed in Fig. 3. One notes that for Cr–Pt film there is a major degradation in the filling factor of the cell (0.63 versus 0.42), which implies an increase in the internal resistivity of the cell. The resistivities of the cells were traced using EIS Nyquist plots (Fig. 3b). The three semi-circles are clearly distinguishable for the FTO–Pt cell; correspond to the charge transfer at the counter electrode (higher frequency, left side), the charge transfer at the TiO_2 interface, and the ionic transport in the electrolyte (low frequency, right side). For the Cr–Pt cell, a large semi-circle appears which corresponds to the interface at the counter electrode and the electrolyte. This large semicircle completely covers the semi-circle related to the TiO_2 interface. The charge transfer resistance values can be easily estimated using circuit models consisting RC elements [56].

The values obtained for the counter electrodes of FTO–Pt and Cr–Pt are 1.1 Ω cm^2 and 23.0 Ω cm^2, respectively. The very large interface charge transfer resistance is caused by the chromium oxide film which is formed and thickened during the Pt thermal decomposition process at 450 °C. This oxide film acts as a barrier for the electron transfer from Pt nanoparticles to the Cr substrate. It is noteworthy to observe that the series resistance of the cell is not increased, and the adverse effect of the oxide film is on the electron transfer processes. The formation of the oxide film and the negative impact on the filling factor and the performance of the cell have been also reported for stainless steel substrates [2,5].

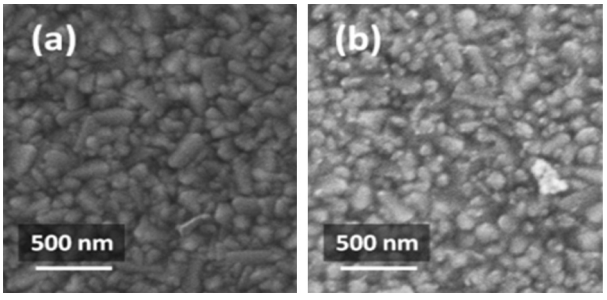

Fig. 2. SEM images of bare FTO surface (a) and Pt thermal deposited FTO (b).

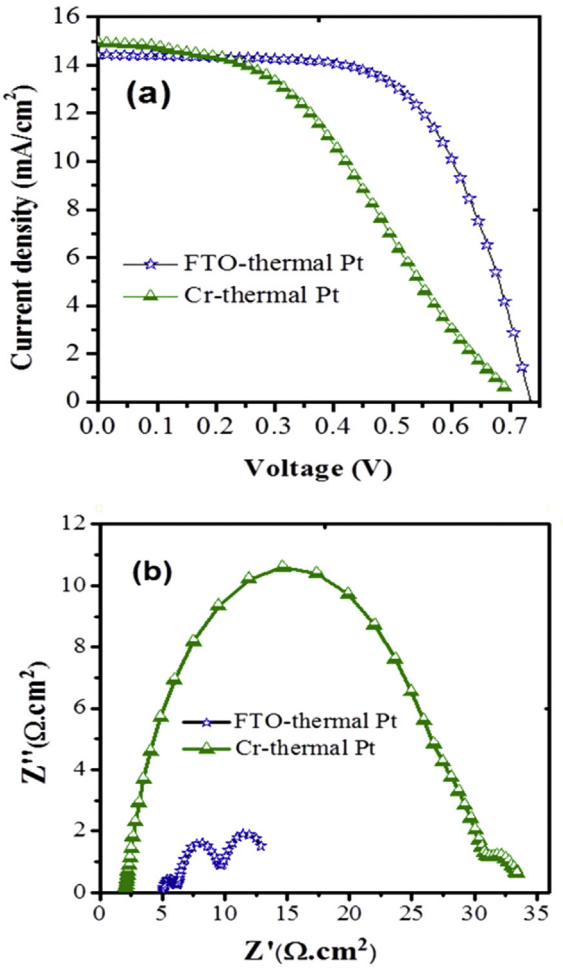

Fig. 3. Comparing current density–voltage (a) and internal resistance (b: Nyquist plot) of DSCs with Pt-deposited FTO and Pt-deposited Cr substrates. Pt was deposited by thermal decomposition method for both cases, and the films were used as the counter electrode of DSCs.

3.2.2. Cyclic electrochemical deposition of Pt

3.2.2.1. The deposition procedure. For the electrochemical deposition of Pt, a low concentration of $H_2PtCl_6 \cdot 6H_2O$ (3 mM) was utilized, due to better growth stability in lower solution concentrations [58]. KNO_3 (50 mM) was used as the supporting electrolyte, as the conventional KCl contains chloride ions, which are corrosive for some metals [59]. Chloride free electrolytes containing an alkaline salt of platinum hydroxide and platinum tetrachloride–phosphate have been already reported for depositing on Ni and stainless steel [60]. The type of supporting electrolyte affects the morphology of the deposited Pt, for instance, it has been shown that by using KCl in cyclic deposition of Pt, irregular shaped Pt nanoparticles are formed on FTO, while $NaNO_3$ results in different shapes such as nanograss and nanoflowers [53]. It is also demonstrated that using SO_4^{2-} ions in a pulse electrodeposition of Pt, nano flower-like Pt structures are produced [52].

In solar cells, the ultimate goal is producing Pt films with the morphology that results in the highest electrocatalytic activity using the lowest quantity of Pt, so we employed a cyclic electrodeposition method for Pt deposition.

The conventional constant voltage electrodeposition produces low density of nuclei, hence low surface area. At a constant voltage,

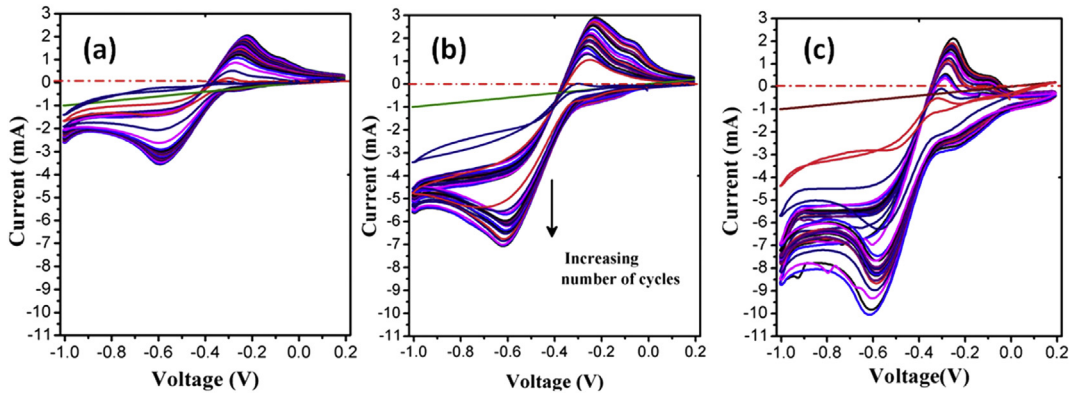

Fig. 4. Cyclic deposition of Pt nanoparticles on Cr substrate: the deposition current of Pt (near −0.6 V) increases with increasing number of cycles. The electrodeposition current increases significantly with increasing the solution temperature from 25 °C (a) to 40 °C (b) and 50 °C (c).

the nuclei are formed at the beginning of the growth, when there is a sufficient supersaturation. Soon after the initial nucleation, a depletion layer is formed and supersaturation drops below that needed to form new nuclei. Therefore, growth continues on the already formed nuclei. Control of the electrodeposition conditions in order to keep supersaturation for more nucleations is very critical for attaining high density of Pt nanoparticles on the surface, in particular cases such as our case where the solution concentration is low. In the cyclic electrodeposition, the flux of ions that diffuse from the bulk to the surface can be controlled by controlling voltage step and scan rate. The current–voltage curve for Pt deposition using cyclic deposition is shown in Fig. 4.

In this Pt deposition, when the potential decreases from 0.2 V, Pt (IV) reduces to Pt (II) and then to the metallic Pt [53]. As the potential is made more negative (down to about −0.6 V), the rate of reduction (Pt(II) to metallic Pt) increases rapidly and Pt nuclei are formed. At a potential slightly more negative than the cathodic peak, the current is controlled by diffusion of ions across the depletion layer to the surface of the electrode. This is diffusion controlled system where the already existing nuclei are grown larger. This is the advantage of the cyclic deposition method to the constant current or constant voltage deposition that in each deposition cycle nucleation and then growth takes place. At higher deposition temperatures the peak current is enlarged and so the nucleation rate increases significantly as shown in Fig. 4.

In the reverse cycle, some of the metallic Pt particles oxidize to Pt (II) and dissolve in the solution [53], hence after a few cycles, the colour of deposition solution becomes darker. The main reaction in the Pt electrochemical deposition is:

$$PtCl_6^{2-}(aq) + 4e^- \rightarrow Pt(s) + 6Cl^-(aq) \quad (1)$$

3.2.2.2. Morphology. SEM images of Pt–Cr films electrodeposited at 40 °C for 5, 10 and 20 cycles, as well as 55 °C for 20 cycles are presented in Fig. 5. One notes that the density of deposited particles increases with the number of cycles (Fig. 5a–c). The cyclic electrodeposition causes new nuclei form in each cycle, in contrast to the constant voltage electrodeposition that leads to the growth of initially formed nuclei. The nanoparticles have a good dispersion on the substrate, and they are hardly agglomerated. However, in average more density of nanoparticles is observed at the edges of the Cr cubes. This can be due to the electric field distribution around the edges. The electric field at sharp locations such as edges is significantly enhanced. There are many growth sites (ledge, kink and ledge-kink sites) on these non-flat edges. For two conductive planes that defines a corner, if the corner angle is 90° and ρ is distance from the intersection of two corners, the surface charge density will be proportional to $\rho^{(-1/3)}$ [60], so there is an accumulation of electrons at the edges of Cr cubes. In contrast, for a deep corner (angle equal to 270°) the surface charge density is proportional to ρ. In case of flat substrates such as FTO the electric field is expected to be uniform.

Comparison of Fig. 5c and d demonstrates the effect of deposition temperature. The density of deposited Pt is increased at 55 °C. This is more clearly observed at the edges where high density of Pt nanoparticles is formed. This is in agreement with the current–voltage data (Fig. 4) which show increased deposition current for higher bath temperatures. Fig. 6 illustrates the SEM images of Pt nanoparticles grown on a FTO substrate with cyclic electrodeposition at 40 °C for 20 cycles.

Comparing the images with similar scale bar, one observes significantly lower number of Pt nanoparticles on the FTO substrate compared to the Cr substrate. Pt particles on FTO are also much

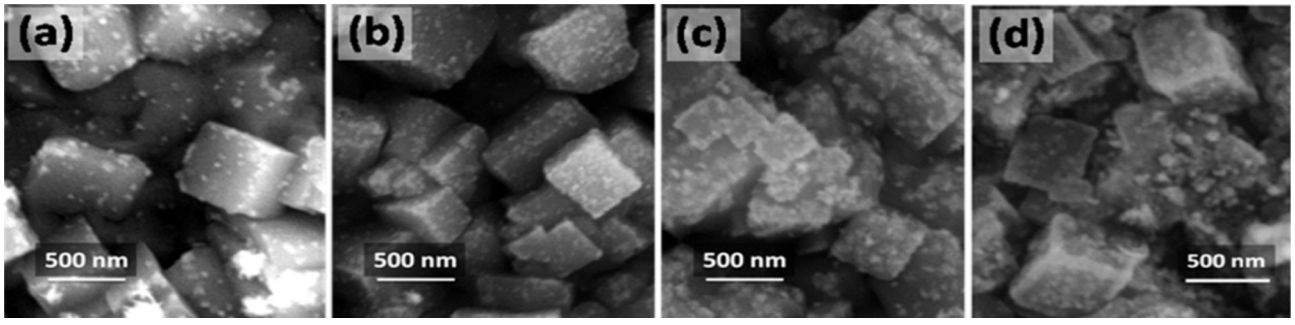

Fig. 5. SEM images of Cr–Pt films. Pt nanoparticles were cyclically electrodeposited at 40 °C for 5 cycles (a), 10 cycles (b), and 20 cycles (c); and 55 °C for 20 cycles (d).

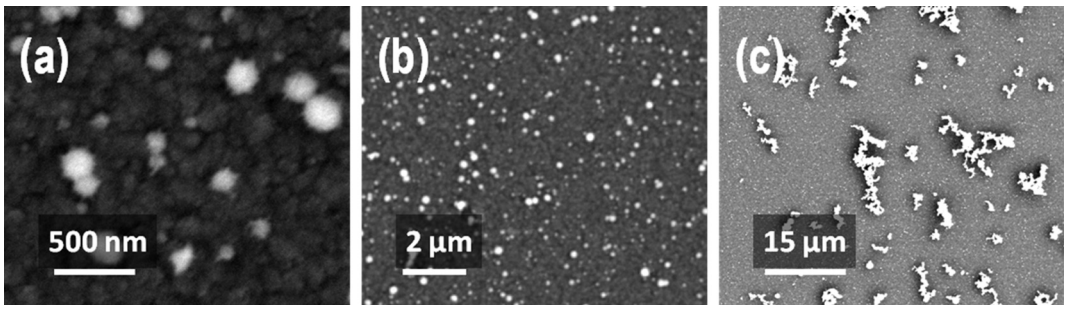

Fig. 6. Images of FTO–Pt films. Pt was cyclically electrodeposited at 40 °C for 20 cycles. Images showing different scales, demonstrate that nuclei are formed in different sizes. At large scale, clusters of Pt nanoparticles are formed during electrodeposition process.

larger. The dispersion of the particles on the surface is also not comparable, especially at a larger scale, where some of these particles join to create clusters of Pt particles (Fig. 6c), this demonstrates that cube-like Cr is a better substrate for of small and dispersed Pt nanoparticles.

3.2.2.3. DSCs with Cr based counter electrode. DSC devices were fabricated using Cr–Pt counter electrodes and were compared with the cells utilizing the conventional FTO–Pt electrodes. Fig. 7 displays the device performance data of the cells having different counter electrodes, and Table 1 summarizes the characteristic data. The photoanode is the same for the cells and consist of a transparent dye sensitized TiO_2 film, without a scattering film. The current–voltage curves in Fig. 7a compare Cr–Pt counter electrodes prepared by cyclic electrodeposition at 25 °C for 5, 10, 15 and 20 deposition cycles. As expected, the open circuit voltage (V_{oc}) is almost unaffected by the type of the counter electrode. The data shows 5 deposition cycles is not sufficient to provide the required low charge transfer resistance. For counter electrodes deposited 10 cycles and more, the device performance is almost identical. However, the problem is the relatively poor filling factor of these cells, i.e. less than 0.6. In principle, the filling factor is a measure of the internal resistivities of the cell.

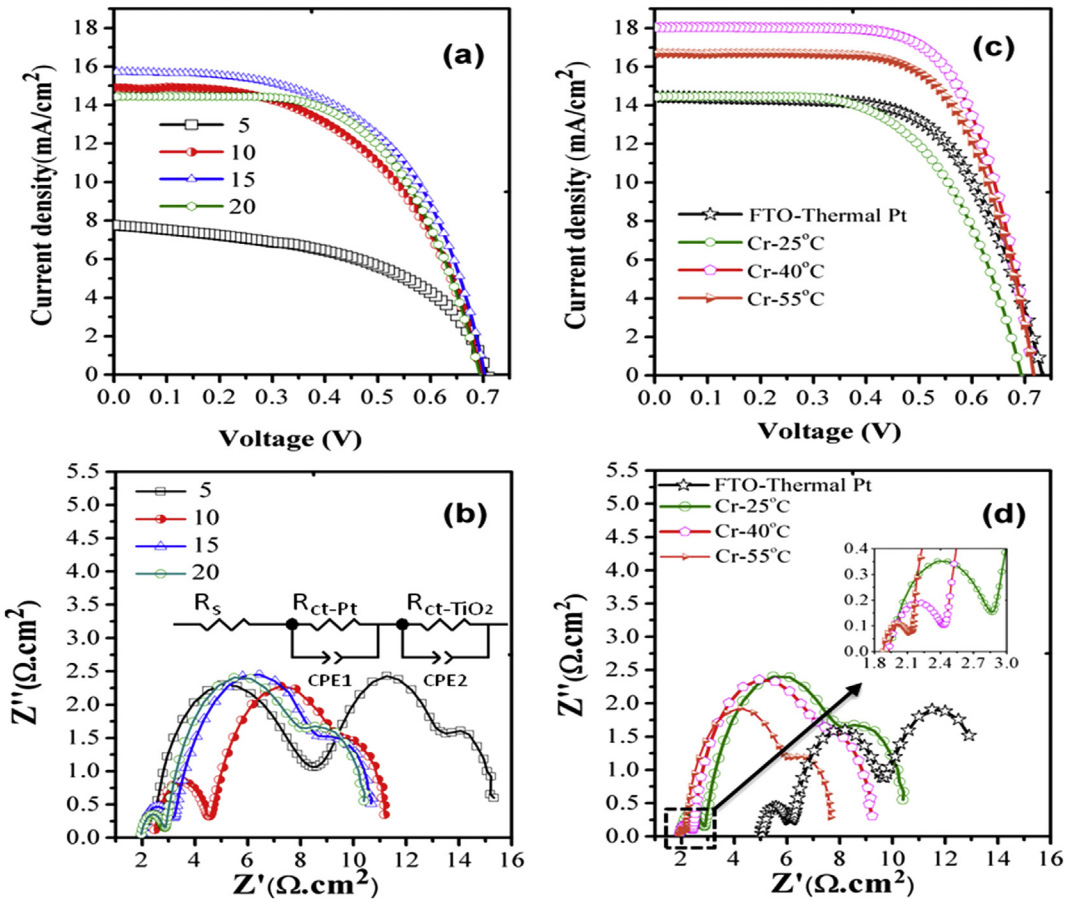

Fig. 7. *J–V* plots (a) and EIS Nyquist plots (b) for DSCs with counter electrodes consisting of Cr substrates cyclically Pt electrodeposited with different number of cycles. Filling factor in-creases by increasing the number of cycles; however current density increases up to 15 cycles and then decreases due to diffuse reflection loss. The size of the first semi-circle in Nyquist plots, corresponding to charge transfer at the counter electrode, becomes smaller with increasing the number of cycles. The effect of deposition temperature (25 °C, 40 °C and 55 °C) on the current density–voltage (c) and on the charge transfer resistance (d) is shown for 20 deposition cycles in comparison with the conventional FTO-thermal counter electrode. No scattering film was used in the photo-anode of the cells, in order to show the effect of diffuse reflection from the surface of counter electrodes.

Table 1
Device parameters of DSCs based on thermal Pt and cyclic electrodeposition on cube-like Cr in comparison with DSC based on conventional FTO-thermal Pt counter electrode. No scattering film was used for the TiO_2 photo-anode. An average for 3 or 4 samples is reported for each case. The characteristics for each sample are reported in the Supplementary information–Extended Table S1.

Substrate	Type of Pt deposition	Deposition temperature (°C)	Number of cycles	R_s (Ω)[a]	$R_{ct,\ Pt}$ (Ω cm^2)	J_{sc} (mA cm^{-2})	V_{oc} (V)	FF	ŋ (%)
FTO	Thermal	450	–	22.9	1.38	14.81	0.720	0.63	6.78
Cr	Thermal	450	–	12.3	13.08	14.00	0.67	0.49	4.73
Cr	Cyclic	25	5	11.25	6.79	12.05	0.67	0.46	3.60
Cr	Cyclic	25	10	11.40	3.99	13.86	0.67	0.50	4.75
Cr	Cyclic	25	15	8.84	2.25	13.72	0.678	0.58	5.45
Cr	Cyclic	25	20	9.90	1.45	14.61	0.660	0.62	6.07
Cr	Cyclic	40	20	10.11	0.54	17.99	0.683	0.69	8.50
Cr	Cyclic	55	20	9.35	0.40	15.76	0.720	0.69	7.81

[a] The series resistance is not normalized to the surface area.

The equivalent resistor elements in the cell can be evaluated by EIS analysis. Fig. 7b displays the Nyquist EIS plots for the mentioned cells. The plots were modelled using the circuit model depicted in the inset of the figure. The first semicircle, at low Z′ values, corresponds to the charge transfer at the Pt counter electrode. The values of charge transfer resistance $R_{ct,\ pt}$ is reported in Table 1. One observes that $R_{ct,\ pt}$ is significantly dependent on the number of cycles. For 5 cycles, $R_{ct,\ pt}$ is 6.79 Ω cm^2 in average, which is generally not appropriate for DSCs. For 20 cycles, $R_{ct,\ pt}$ is 1.45 Ω cm^2 in average.

Fig. 7c and d shows the effect of the electrochemical bath temperature on the performance of the corresponding cells. Reference cells utilizing FTO-thermal Pt counter electrodes are used for a comparison. Cr–Pt counter electrodes were prepared by a cyclic electrodeposition for 20 cycles at 25 °C, 40 °C and 55 °C. The *J–V* plots clearly show the remarkable role of deposition temperature on the performance of the cells.

The highest device performance is obtained for 40 °C deposition temperature: J_{sc} = 18.0 mA cm^{-2}, V_{oc} = 0.715 V, FF = 0.68 and conversion efficiency η = 8.77%. One should note that no scattering film was used in the cell. The diffuse reflection of Cr surface is lower than that of TiO_2 scattering layer (for example with size of 150–250 nm and anatase phase) in air, but the diffuse reflection of TiO_2 scattering layer decreases significantly inside the electrolyte in dye solar cells down to about 50% due to decreasing the refractive index contrast of TiO_2 and the surrounding medium [61], therefore it seems Cr films do relatively similar back-reflection function as the conventional large TiO_2 back reflector films.

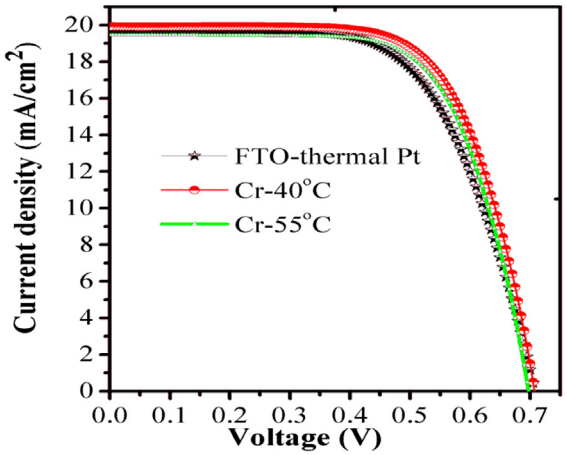

Fig. 8. The current density–voltage curves for DSCs with Cr–Pt counter electrodes, compared to the conventional FTO-thermal Pt electrode. Pt nanoparticles on the cube-like Cr film were deposited by cyclic electrodeposition at 40 °C and 55 °C. The cells were fabricated using a TiO_2 photoanode containing a scattering film. The effect of counter electrodes in these optimized conditions is only on the filling factor.

For 55 °C, the cell shows slightly lower current density. This is mainly due to the relatively darker appearance of the counter electrode, which reduces the intensity of back-reflected light from the surface of Cr–Pt electrode. For the reference cell with FTO–Pt counter electrode, J_{sc} is lower possibly due to the less back-reflected light (FTO–Pt is almost transparent), and FF is slightly inferior presumably due to a larger $R_{ct,\ pt}$ and R_s (series resistance). The charge transfer resistance can be also the main differentiating factor for 40 °C and 55 °C cells compared to the 25 °C cell. The values of $R_{ct,\ pt}$ and R_s were measured by the EIS plots (Fig. 7d), and tabulated in Table 1. The charge transfer resistance at the counter electrode, $R_{ct,\ pt}$, becomes remarkably low for Cr–Pt electrodes prepared at 40 °C and 55 °C; i.e. as low as 0.27 Ω cm^2. This is the reason for the greatly improved conversion efficiency of the Cr-based cells.

Higher current peak and small potential difference as low as 0.2 V between anodic and cathodic current peak in cyclic voltammograms (that are obtained in iodide based electrolyte), show high electro–catalytic activity of these new counter electrodes (Supplementary information–Fig. S3).

Fig. 8 shows the *J–V* plots for the optimized DSCs utilizing a scattering back-reflector film. Cr–Pt counter electrodes of 40 °C/20 cycles and 50 °C/20 cycles are compared with FTO–Pt films prepared using the conventional thermal decomposition method. Table 2 summarizes the device performance data. J_{sc} and V_{oc} of the cells are almost similar, with Cr–Pt-40 °C showing the highest J_{sc} (19.93 mA cm^{-2}) and FTO–Pt showing the highest V_{oc} (0.710 V). The main differentiating factor is the filling factor which is 0.68 for Cr-based cells and 0.63 for FTO-based cells. This again confirms the claim that using Cr–Pt electrode reduces the internal resistance of the cell. A conversion efficiency as high as 9.52% is obtained with Cr–Pt cells.

The highest device performance is obtained for 40 °C deposition temperature: J_{sc} = 18.0 mA cm^{-2}, V_{oc} = 0.715 V, FF = 0.68 and conversion efficiency η = 8.77%. One should note that no scattering film was used in the cell. For 55 °C, the cell shows slightly lower

Table 2
Device parameters for DSCs with Cr–Pt counter electrode in comparison with DSC with conventional FTO-thermal Pt counter electrode. A scattering film is used in the photo-anodes. An average for 3 or 4 samples is reported for each case. The characteristics for each sample are reported in the Supplementary information-Extended Table S2.

Substrate	Type of deposition	Deposition temperature (°C)	Number of cycles	J_{sc} (mA cm^{-2})	V_{oc} (V)	FF	ŋ (%)
FTO	Thermal	450	–	19.64	0.707	0.630	8.71
Cr	Cyclic	40	20	19.73	0.693	0.692	9.24
Cr	Cyclic	55	20	19.59	0.693	0.694	9.49

current density. This is mainly due to the relatively darker appearance of the counter electrode, which reduces the intensity of back-reflected light from the surface of Cr–Pt electrode (IPCE spectra-Supplementary information, Fig. S4). For the reference cell with FTO–Pt counter electrode, J_{sc} is lower possibly due to the less back-reflected light (FTO–Pt is almost transparent), and FF is slightly inferior presumably due to a larger $R_{ct,\ pt}$ and R_s (series resistance). The charge transfer resistance can be also the main differentiating factor for 40 °C and 55 °C cells compared to the 25 °C cell. The values of $R_{ct,\ pt}$ and R_s were measured by the EIS plots (Fig. 7d), and tabulated in Table 1.

4. Conclusion

A novel counter electrode consisting of an electroplated cube-like chromium substrate and cyclically electrodeposited Pt nanoparticles is introduced for DSCs. The cube-like Cr substrate shows a cubic morphology with a high surface area, suitable for depositing dispersed Pt nanoparticles. It also provides very low sheet resistance compared to FTO, which considerably reduces the series resistance of the cells. We have demonstrated that the charge transfer resistance at the Pt electrode can be as low as 0.27 Ω cm^2 for cyclically electrodeposited Pt films on cube-like Cr film. The Cr–Pt film electro-deposited at 40 °C for 20 cycles, shows the highest conversion efficiency of 8.77% without a scattering film and 9.52% with a scattering film. The results prove the feasibility of replacing the conventional expensive FTO substrates with Cr electroplated conductive layers or foils. This is expected to reduce the fabrication cost and improve the device performance by decreased series and internal resistance of the cells, particularly for large cells and modules. The process being near room temperature, makes it possible to use flexible metal foils or conductive plastics as the substrate of DSCs. The method is, in principle, applicable to other substrates including ITO/PEN or metal foils, with some considerations on the stability in the Cr electroplating bath, as well as the adhesion concerns.

Appendix A. Supplementary data

Supplementary data related to this article can be found at http://dx.doi.org/10.1016/j.jpowsour.2014.02.074.

References

[1] B. Oregan, M. Gratzel, Nature 153 (1991) 737–740.
[2] T. Ma, X. Fang, M. Akiyama, K. Inoue, H. Noma, E. Abe, J. Electroanal. Chem. 574 (2004) 77–83.
[3] K. Okada, H. Matsui, T. Kawashima, T. Ezure, N. Tanabe, J. Photochem. Photobiol. A Chem. 164 (2004) 193–198.
[4] G.J. Reynolds, T.M. Watson, G. Williams, D.A. Worsley, ECS Trans. 33 (2011) 129–138.
[5] M. Toivola, F. Ahlskog, P. Lund, Sol. Energy Mater. Sol. Cells 90 (2006) 2881–2893.
[6] M. Wu, T. Ma, ChemSusChem 5 (2012) 1343–1357.
[7] K. Miettunen, J. Halme, M. Toivola, P. Lund, J. Phys. Chem. C 112 (2008) 4011–4017.
[8] X. Fan, F. Wang, Z. Chu, L. Chen, C. Zhang, D. Zou, Appl. Phys. Lett. 90 (2007) 073501-1–073501-3.
[9] X. Huang, P. Shen, B. Zhao, X. Feng, S. Jiang, H. Chen, H. Li, S. Tan, Sol. Energy Mater. Sol. Cells 94 (2010) 1005–1010.
[10] M.G. Kang, N.G. Park, K.S. Ryu, S.H. Chang, K.J. Kim, Sol. Energy Mater. Sol. Cells 90 (2006) 574–581.
[11] J.H. Park, Y. Jun, H.G. Yun, S.Y. Lee, M.G. Kang, J. Electrochem. Soc. 155 (2008) F145–F149.
[12] C.M. Chen, C.H. Chen, T.C. Wei, Electrochim. Acta 55 (2010) 1687–1695.
[13] N. Fuke, A. Fukui, R. Komiya, A. Islam, Y. Chiba, M. Yanagida, R. Yamanaka, L. Han, Chem. Mater. 20 (2008) 4974–4979.
[14] D. Fu, P. Lay, U. Bach, Energy Environ. Sci. 6 (2013) 824–829.
[15] T.Y. Tsai, C.M. Chen, S.J. Cherng, S.Y. Suen, Prog. Photovolt. Res. Appl. 21 (2011) 226–231.
[16] C.S. Rustomji, Ch J. Frandsen, S. Jin, M.J. Tauber, J. Phys. Chem. B 114 (2010) 14537–14543.
[17] G. Veerappan, K. Bojan, S.W. Rhee, ACS Appl. Mater. Interfaces 3 (2011) 857–862.
[18] A. Kay, M. Gratzel, Sol. Energy Mater. Sol. Cells 44 (1996) 99–117.
[19] F. Malara, M. Manca, L.D. Marco, P. Pareo, G. Gigli, ACS Appl. Mater. Interfaces 3 (2011) 3625–3632.
[20] S.J. Thompson, N.W. Duffy, U. Bach, J. Phys. Chem. C 114 (2010) 2365–2369.
[21] B. Lee, D.B. Buchholz, R.P.H. Chang, Energy Environ. Sci. 5 (2012) 6941–6952.
[22] J. Chen, F. Meng, X. Gui, H. Sun, Z. Zeng, Z. Li, Y. Zhou, Z. Tang, Carbon 50 (2012) 5618–5630.
[23] X. Fang, T. Ma, M. Akiyama, G. Guan, S. Tsunematsu, E. Abe, Thin Solid Films 472 (2005) 242–245.
[24] K. Miettunen, J. Halme, P. Lund, WIREs Energy Environ. 2 (2013) 104–120.
[25] A.F. Kanta, A. Decroly, Mater. Chem. Phys. 130 (2011) 843–846.
[26] Q.W. Jiang, G.R. Li, X.P. Gao, Chem. Commun. (2009) 6720–6722.
[27] M.X. Wu, X.A. Lin, A. Hagfeldt, T.L. Ma, Chem. Commun. 47 (2011) 4535–4537.
[28] M.X. Wu, X.A. Lin, A. Hagfeldt, T.L. Ma, Angew. Chem. Int. 134 (2011) 3520–3524.
[29] M. Wu, X. Lin, Y. Wang, L. Wang, W. Guo, D. Qi, X. Peng, A. Hagfeldt, M. Gratzel, T. Ma, J. Am. Chem. Soc. 134 (2012) 3419–3428.
[30] H. Sun, D. Qin, S. Huang, X. Guo, D. Li, Y. Luo, Q. Meng, Energy Environ. Sci. 4 (2011) 2630–2637.
[31] S. Yun, M. Wu, Y. Wang, J. Shi, X. Lin, A. Hagfeldt, T. Ma, ChemSusChem 6 (2013) 411–416.
[32] Y. Saito, T. Kitamura, Y. Wada, S. Yanagida, Chem. Lett. 31 (2002) 1060–1061.
[33] Y. Saito, W. Kubo, T. Kitamura, Y. Wada, S. Yanagida, J. Photochem. Photobiol. A. Chem. 164 (2004) 153–157.
[34] M. Wu, X. Lin, T. Wang, J. Qiub, T. Ma, Energy Environ. Sci. 4 (2011) 2308–2315.
[35] W. Kwon, J.M. Kim, S.W. Rhee, J. Mater. Chem. A 1 (2013) 3202–3215.
[36] T.N. Murakami, M. Gratzel, Inorg. Chim. Acta 361 (2008) 572–580.
[37] M. Liang, W. Xu, F. Cai, P. Chen, B. Peng, J. Chen, Z. Li, J. Phys. Chem. C 111 (2007) 4465–4472.
[38] J.Y. Lin, Y.T. Lin, Surf. Coat. Technol. 206 (2012) 4672–4678.
[39] N.Q. Fu, X.R. Xiao, X.W. Zhou, J.B. Zhang, Y. Lin, J. Phys. Chem. C 116 (2012) 2850–2857.
[40] X.L. He, M. Liu, G.J. Yang, S.Q. Fan, C.J. Li, Appl. Surf. Sci. 258 (2011) 1377–1384.
[41] Y. Jun, J. Kim, M.G. Kang, Sol. Energy Mater. Sol. Cells 91 (2007) 779–784.
[42] L. Matoh, I.K. Škofic, M. Čeh, N. Bukovec, J. Mater. Chem. A 1 (2013) 1065–1069.
[43] N.Q. Fu, Y.Y. Fang, Y.D. Duan, X.W. Zhou, X.R. Xiao, Y. Lin, ACS Nano 6 (2012) 9596–9605.
[44] X. Fang, T. Ma, G. Guan, M. Akiyama, T. Kida, E. Abe, J. Electroanal. Chem. 570 (2004) 257–263.
[45] G. Syrrokostas, A. Siokou, G. Leftheriotis, P. Yianoulis, Sol. Energy Mater. Sol. Cells 103 (2012) 119–127.
[46] C.Y. Lin, J.Y. Lin, C.C. Wan, T.C. Wei, Electrochim. Acta 56 (2011) 1941–1946.
[47] S.S. Kim, Y.C. Nah, Y.Y. Noh, J. Jo, D.Y. Kim, Electrochim. Acta 51 (2006) 3814–3819.
[48] P. Li, J. Wu, J. Lin, M. Huang, Z. Lan, Q. Li, Electrochim. Acta 53 (2008) 4161–4166.
[49] C.C. Yang, H.Q. Zhang, Y.R. Zheng, Curr. Appl. Phys. 11 (2011) S147–S153.
[50] D. Fu, P. Huang, U. Bach, Electrochim. Acta 77 (2012) 121–127.
[51] Y.J. Song, J.K. Oh, K.W. Park, Nanotechnology 19 (2008) 355602-1–355602-6.
[52] T.L. Hsieh, H.W. Chen, C.W. Kung, C.C. Wang, R. Vittal, K.C. Ho, J. Mater. Chem. 22 (2012) 5550–5559.
[53] L.L. Li, C.W. Chang, H.H. Wu, J.W. Shiu, P.T. Wu, E.W.G. Diau, J. Mater. Chem. 22 (2012) 6267–6273.
[54] V.D. Dao, S.H. Kim, H.S. Choi, J.H. Kim, H.O. Park, J.K. Lee, J. Phys. Chem. C 115 (2011) 25529–25534.
[55] F. Hao, H. Lin, Y. Liu, N. Wang, W. Li, J. Li, ACS Appl. Mater. Interfaces 3 (2011) 3916–3920.
[56] H.G. Yun, Y. Jun, J. Kim, B.S. Bae, M.G. Kang, Appl. Phys. Lett. 93 (2008) 133311-1–133311-3.
[57] C.H. Tsai, S.Y. Hsu, C.Y. Lu, Y.T. Tsai, T.W. Huang, Y.F. Chen, Y.H. Jhang, C.C. Wu, Org. Electron. 13 (2012) 199–205.
[58] G.Z. Cao, Y. Wang, Nanostructures and Nanomaterials: Synthesis, Properties, and Applications, Imperical College Press, Weinheim, 2004.
[59] C.R.K. Rao, D.C. Trivedi, Coord. Chem. Rev. 249 (2005) 613–631.
[60] J.D. Jackson, Classical Electrodynamics, John Wiley and Sons, NewYork, 1999.
[61] N. Ghazyani, M. Majles Ara, F. Tajabadi, A. Dabirian, R. Mohammadpour, N. Taghavinia, RSC Adv. (2013), http://dx.doi.org/10.1039/C3RA44079F.